Characterisation of Fracture Permeability at Cow Lagoon-1, McArthur Basin, Northern Territory, Australia and Recommendations for Development of the Greater Cow Lagoon Structure.

Scott Mildren, Ikon Science, Rachael Clark, Australian School of Petroleum, Simon Holford, Australian School of Petroleum, Luke Titus, Armour Energy

Abstract

Resistivity image log interpretation of Armour Energy's Cow Lagoon-1 well in the Batten Trough of the McArthur Basin identified conductive and resistive fractures and faults throughout the interval. The 423 fracture surfaces and 55 faults interpreted display a dominant strike direction approximately 150°N and secondary fracture populations striking east-west around 060°N. Two borehole breakouts were also determined from image logs and used to constrain the mean maximum horizontal stress direction to 133°N. Contemporary stress distribution in the well is variable and fundamentally linked to the elastic properties of the sampled stratigraphy. Both strike-slip and extensional regimes are represented by the data.

Fracture susceptibility models indicate that the minimum ΔP to initiate a fracture is relatively high in all formations and generally exceeds 25 MPa. This reflects high strength calculated for these units and implies that creation of new fractures under the contemporary stress conditions is unlikely. Reactivation of existing fracture planes is more likely, with minimum ΔP < 7 MPa in each model generated.

Fracture density was shown to vary across the interpreted interval and also strongly correlates with stratigraphy. Steeper bedding dips consistently correlate with an increase in fracture density. Fault count was attributed to the stress conditions and modes of failure. Low fault count correlates with tensile failure, whilst high fault count implies shear failure.

Systematic analysis of the Cow Lagoon-1 data concludes that NNW striking fractures are critically oriented for shear reactivation in the far field stress environment within the Upper Lynott and Reward Formations. Such fractures correspond with high fault density and preferentially occur within low strength, low Young's Modulus and low differential and effective stress units.

Introduction

Fracture networks are fundamental to hydrocarbon production within many unconventional resources. Structural permeability in these scenarios can be attributed to existing natural fracture networks, placement of fracture networks through injection operations, or a combination of the two. In addition, natural fracture permeability and placement of hydraulic fractures has been demonstrated to be intrinsically linked to the contemporary stress field (Sibson, 1996). Constraint of principal stress magnitudes and orientations within the subsurface permits ranking of observed natural fracture populations and identification of stress conditions conducive to complex fracture placement. Beyond unconventional permeability, constraint of a geomechanical model can also benefit these projects by optimising well placement, maximizing wellbore stability and providing insight into reservoir flooding and drainage patterns (Hillis and Reynolds, 2003; Hillis et al. 2000).

Armour Energy drilled Cow Lagoon-1 on the Cow Lagoon West Anticline within the Batten Trough of the McArthur Basin in Australia's Northern Territory in 2012. The well encountered gas from the Mid-Proterozoic Lynott and Reward Formations and further shows were recorded in the similarly aged Barney Creek Shale. Resistivity image log data was acquired from the well and cursory assessment indicated the presence of fractures. Stresses are redistributed around wellbores once they are

drilled and observations made at the wellbore wall may not necessarily reflect the influence of the far-field stress environment. This study was undertaken to constrain the in situ stress tensor at Cow Lagoon-1 and use it to assess the fracture observations made from the acquired image log. The fundamental objective was to characterise fracture distribution, assess the permeability of these structural elements and explore options for production.

Geological Background

The Cow Lagoon prospect is located within the Batten Trough of the McArthur Basin, Northern Territory, Australia. The basin covers an area of approximately 180,000km^2 (Figure 1). It extends with a N-NW trend from the Queensland-Northern Territory border, along the west coast of the Gulf of Carpentaria, to the north coast of Arnhem Land (Rawlings *et al.,* 2002). The basin is divided tectonically into the North and South McArthur Basin, which is crosscut by the East-West trending Urapunga fault zone. The north and south of the basin are also bisected by two 50-80km wide structural corridors that trend N-S and have been termed the Walker and Batten fault zones respectively (Rawlings *et al.,* 2002). The McArthur Basin is generally regarded to have developed under an extensional regime (Edgoose *et al.* 2013) with McArthur Group sediments deposited during the Palaeoproterozoic.
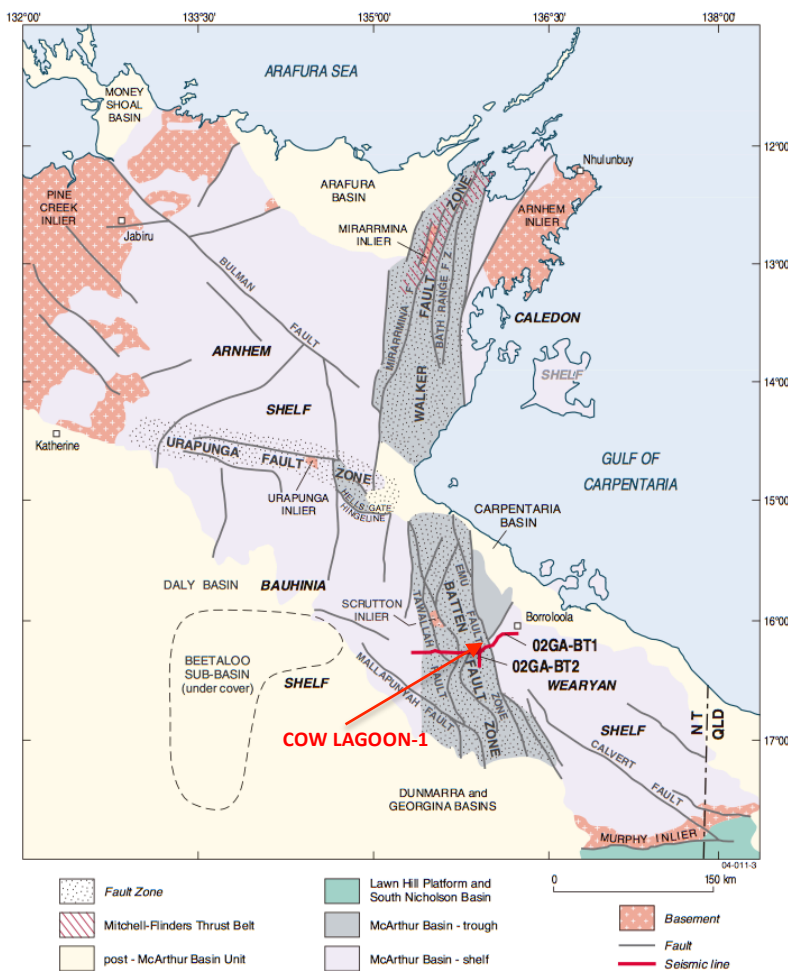
Figure 1: Geological map showing the extent of the McArthur Basin, present structural regions and the location of Cow Lagoon-1 (adapted from Rawlings, 2002b; Rawlings *et al.* 2002).

Available Data

A resistivity image log and a full suite of wireline logs were acquired at Cow Lagoon-1. These were run from TD (1804.9m) to the first casing shoe (238.6m), covering the majority of the drilled interval. Density logs were run to the surface. The image log data was acquired using Weatherford's 8-arm Compact microimager (CMI) tool which was run in an 8 ½" hole, allowing for good coverage of the wellbore wall.

Three coring runs were taken at depth intervals of 586.3-589.0mMD, 753.1-761.5mMD and 1356.0-1357.2mMD. Full core descriptions were available, but as yet no laboratory testing has been performed.

The well was initially drilled using conventional methods utilising KCL drilling fluids weighted close to pore pressure. The 8 ½" hole was drilled underbalanced using air hammer methods, with air/mist as the drilling fluid. An arbitrary figure of 2ppg was used as an estimate of mud weight for this section. Coring and logging intervals were conducted with 8.5ppg KCL drilling fluid in the hole. Pore pressure was assumed to be normal density seawater at 8.5ppg.

A formation integrity test (FIT) was conducted at 239 m, but no further testing was acquired within the well.

Image Log Interpretation

Image log interpretation consisted of identifying simple bedding surfaces, faults, fractures and in situ stress indicators such as borehole breakouts and drilling induced tensile fractures (DITF; Table 1). Bedding surfaces are distinguished from structural features based on cross cutting relationships. Classification of faults and fractures was based on resistivity response (conductive or resistive) and wellbore morphology (discontinuous, continuous and full wellbore surfaces).

Far-field stresses are redistributed around a wellbore to re-equilibrate following the removal of rock by the drilling process. A borehole breakout is indicative of compressive failure at the wellbore wall where the circumferential stress has exceeded the

rock strength. This deformation is observed at azimuths perpendicular to the maximum horizontal stress direction within vertical wells. Breakouts appear as electrically conductive areas on resistivity image logs which commonly coincide with a cessation of tool rotation and elongated caliper arms. A drilling induced tensile fracture occurs at azimuths parallel to the maximum horizontal stress direction where the circumferential stress is reduced and exceeds the tensile strength of the wall rock. DITF's do not propagate significantly into the surrounding rocks and in vertical wells are axial to the wellbore. They are typically no longer than 2m and display small jogs or kinks (Brudy and Zoback, 1999).

Table 1: Classification scheme used for image log interpretation of Cow Lagoon-1.

Classification	Description
Bed	Basic bedding surface observed as a full sinusoid around the wellbore image.
BO	Borehole breakout. Conductive zone axial to borehole and observed on opposing sides of wellbore separated by 180º.
DITF	Drilling induced tensile fracture, vertical, displayed on two sides of wellbore separated by 180º.
CFracF	Conductive surface cross-cutting bedding surfaces and observed around entire wellbore image.
CFracC	Conductive surface cross-cutting bedding surfaces and continuously present around a proportion of the wellbore wall.
CFracD	Conductive surface cross-cutting bedding surfaces and discontinuously observed around the wellbore wall.
RFracF	Resistive surface cross-cutting bedding surfaces and observed around entire wellbore image.
RFracC	Resistive surface cross-cutting bedding surfaces and continuously present around a proportion of the wellbore wall.
RFracD	Resistive surface cross-cutting bedding surfaces and discontinuously observed around the wellbore wall.
CFaultF	Conductive surface displacing bedding surfaces and observed around entire wellbore image.
CFaultC	Conductive surface displacing bedding continuous sinusoid around wellbore image.
CFaultD	Conductive surface displacing bedding discontinuous sinusoid around wellbore image.
RFaultF	Resistive surface displacing bedding surfaces and observed around entire wellbore image.
RFaultC	Resistive surface displacing bedding surfaces and continuously present around a proportion of the wellbore wall.
RFaultD	Resistive surface displacing bedding surfaces and discontinuously observed around the wellbore wall.

Fracture Characterisation

423 fracture surfaces and 55 faults were identified from the Cow Lagoon-1 image log and these surfaces are summarised in Table 1, Table 2, Figure 2 and Figure 3. The greatest proportion of structural surfaces identified from the interpreted interval was classified as discontinuous conductive fractures (46%) and continuous conductive fractures (38%). The dominant strike direction observed for all fractures and fault populations is approximately 150°N. Secondary populations are also observed striking east-west and around to 060°N (Figure 3). This population is almost exclusively classified as discontinuous conductive fractures (CfracD). Relatively few resistive fractures were identified and those that were are sub-parallel to the primary conductive strike direction (140°N). Dip magnitude of all structural surfaces are relatively high averaging above 50° for nearly all classification types. Localised increases in dip magnitude reach 70-80°. The dominant NNW strike of these fracture populations is consistent with the most significant structural feature in the region, the Batten Fault Zone.

Fracture density varies across the interpreted interval and strongly correlates with stratigraphy (Figure 2). The Leila Sandstone, Myrtle Shale and Mara Member at the base of the interval each have relatively low fracture densities. The base of the Mara Member coincides with a dramatic increase in dip magnitude from <10° up to approximately 70° within the overlying Mitchell Yard Dolomite. The depth at which the maximum dip is observed also coincides with a dramatic increase in fracture density. Bedding gradually decreases within this formation and dip magnitudes of 10-20° are observed within the overlying Lower Teena and Coxco Dolomites. Conductive fracture density is maximized within these two units and the average dip magnitude of these surfaces increases beyond 70°.

The Barney Creek Formation and the lower 100m of the overlying Reward Dolomite are relatively fracture free with consistent low angle bedding towards the northwest. At approximately 1100m, bedding surface orientations are more variable and begin to systematically increase in dip magnitude. This also coincides with increasing conductive fracture density. Dip magnitude of bedding surfaces reaches a maximum at 1000m (45°) before reducing again. There is a secondary increase in dip magnitude between 900-950m, which coincides with a dramatic increase in observed fault surfaces.

The overlying undifferentiated Lynott Formation is characterized by bedding surfaces predominantly dipping <= 50° with the exception of short intervals with localized dip increases. Fracture and fault density through this formation remains elevated up to approximately 400m.
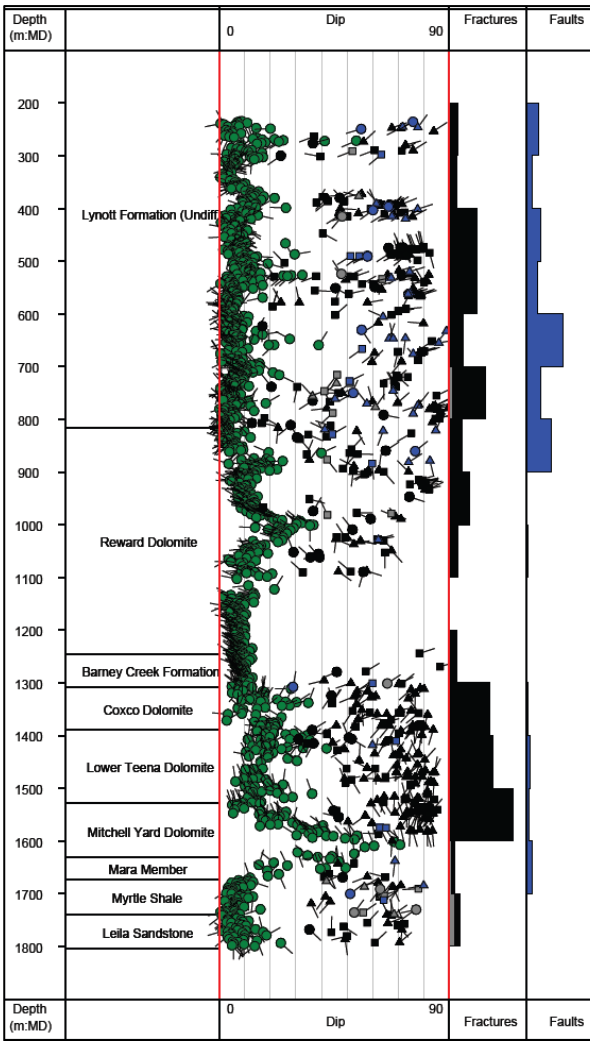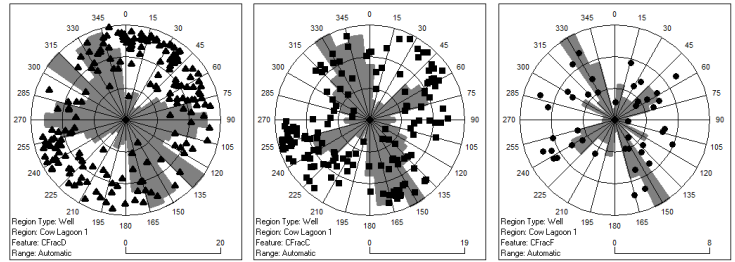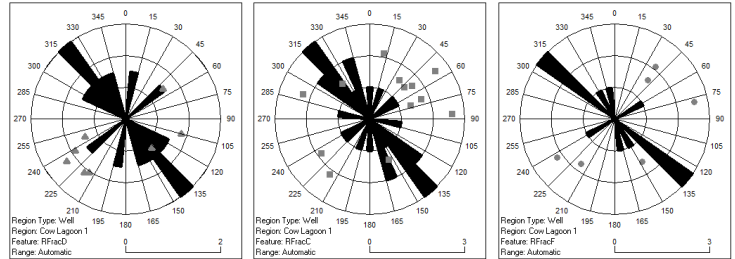
Figure 2: Depth vs. dip plot showing bedding (green), conductive fractures (black), resistive fractures (grey) and faults (blue) for the Cow Lagoon-1 well.
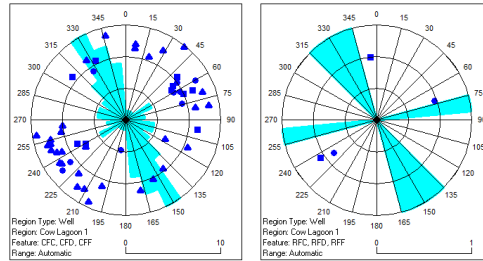

Figure 3: Rose plots displaying data interpreted from the Cow Lagoon-1 image log. Plots show: A - conductive fractures (left to right: CFracD, CFracC and CFracF); B - resistive fractures (left to right: RFracD. RFracC and RFracF) and; C - conductive and resistive faults (left to right: CFaultC, CFaultD, CFaultF and RFaultC, RFaultD, RFaultF). Fracture and fault populations are plotted as poles to planes.

Table 2: Summary of surfaces identified from the Cow Lagoon-1 image log calculated using directional and vector statistics where Count is the number of surfaces, Dip is the mean dip magnitude, Dip Dirn. is the mean dip direction and SD is the respective standard deviation of the mean. Raw and corrected average densities for the interpreted interval are also provided for each surface type (fracs/m).

Surface Type	Count	Directional Statistics					Vector Statistics			Density	
		Dip (°)	SD (°)	Dip Dirn (°N)	SD (°)	Strike (°N)	SD (°)	Dip (°)	Dip Dirn (°N)	Raw	Cor.
CFracD	193	68	13.0	194	104.5	126	45.1	26	193	0.123	0.453
CFracC	161	62	17.3	039	110.1	155	52.0	16	044	0.103	0.334
CFracF	42	47	17.0	270	147.4	004	58.4	3	067	0.027	0.049
RFracC	13	56	12.7	227	81.0	145	37.5	28	226	0.008	0.017
RFracD	8	54	10.5	021	70.9	148	31.5	34	026	0.005	0.010
RFracF	6	59	10.6	288	97.2	137	31.0	21	284	0.004	0.009
CFaultD	32	70	10.2	054	94.2	144	40.9	36	058	0.020	0.091
CFaultC	9	58	7.7	201	79.9	153	30.2	34	203	0.006	0.011
CFaultF	9	59	13.4	245	94.8	145	27.3	24	238	0.006	0.013
RFaultD	0	-	-	-	-	-	-	-	-	-	-
RFaultC	3	60	3.5	174	83.8	130	30.6	30	169	0.002	0.004
RFaultF	2	55	3.4	332	109.3	152	9.4	13	318	0.001	0.002

The Cow Lagoon In-Situ Stress Tensor

The stress tensor can be determined by constraining the orientation and magnitude of the three principal stresses denoted σ_1, σ_2, σ_3. The vertical stress (σ_v) is assumed to be a principal stress thereby constraining the two remaining principal stresses to the horizontal plane; minimum horizontal stress (σ_h), and maximum horizontal stress (σ_H). The full stress tensor is then defined by the orientation of the two horizontal stresses and by the magnitude of all three (Hillis *et al.* 2000). Relative magnitudes of the principal stresses define what the stress regime is; whether it is extensional ($\sigma_v > \sigma_H > \sigma_h$); strike-slip ($\sigma_H > \sigma_v > \sigma_h$) or; compressional ($\sigma_H > \sigma_h > \sigma_v$).

Observations of borehole breakout and drilling induced tensile fractures from image logs were used to constrain the orientation of the two horizontal principal stresses. Two borehole breakouts and no DITF were identified within the Cow Lagoon-1 image log (Figure 4 and Figure 5). Each borehole breakout was relatively short and both are considered to be low quality with a mean maximum horizontal stress direction oriented 133°N.
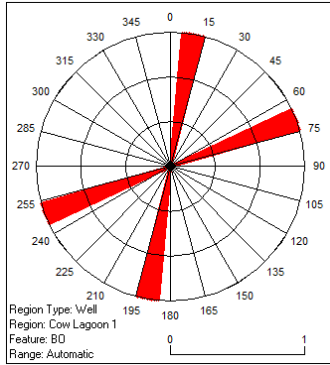
Figure 4 (above): Rose plot showing strike orientations of BO.

Figure 5 (right): Image log section showing BO from 1169.6 to 1169.9m.
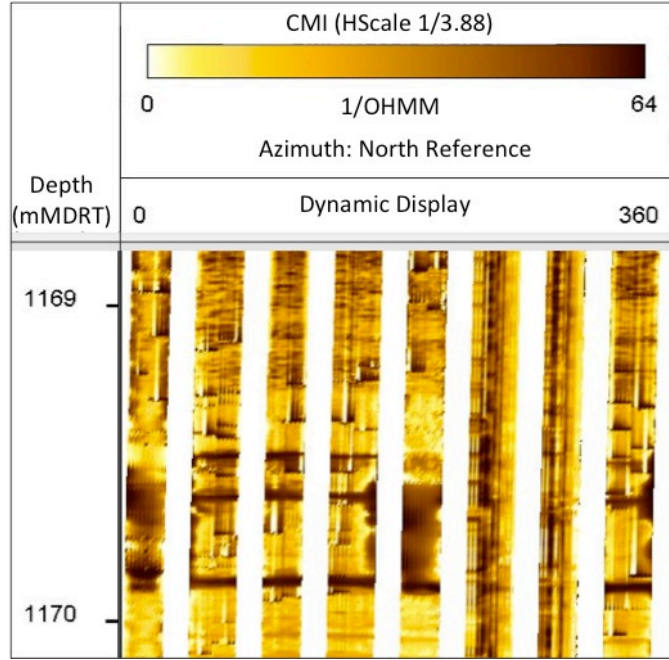
The magnitude of vertical stress is effectively the weight of the overburden and can therefore be determined by the integration of a density curve from the well of interest, such that:

$$\sigma_v = \int\limits_0^z \rho(z)g\,dz$$

where z is the vertical depth, $\rho(z)$ is the function of density with depth and g is the acceleration due to gravity (Zoback 2007). This calculation was performed for Cow Lagoon-1 and is illustrated in Figure 6.

No leakoff or minifrac tests were performed at Cow Lagoon-1 and therefore no direct measurements of the minimum horizontal stress magnitude were made. However, a sole formation integrity test to 3.8MPa was performed at 243.0mMD and this measurement is considered to be a lower bound to σ_h magnitude.

Continuous log derived estimates of σ_h and σ_H magnitude were made by solving linear poroelastic equations for horizontal stresses, which take into account estimates for tectonic strain (Blanton and Olson, 1999):

$$\sigma_h = \frac{v}{1-v}\left(\sigma_v - \alpha.Pp\right) + \frac{E}{1-v^2}.\varepsilon_h + \frac{Ev}{1-v^2}.\varepsilon_H + \alpha.Pp$$

$$\sigma_H = \frac{v}{1-v}\left(\sigma_v - \alpha.Pp\right) + \frac{E}{1-v^2}.\varepsilon_H + \frac{Ev}{1-v^2}.\varepsilon_h + \alpha.Pp$$

where v is the poisson's ratio, σ_v is the vertical stress, α is Biot's constant, Pp is the pore pressure, E is Young's Modulus, ε_h is the strain in the direction of σ_h and ε_H is the strain in the direction of σ_H. Elastic properties for use in these equations were also derived from log data and dynamic to static calibrations were applied. Laboratory tests of core samples were unavailable and therefore further calibration of these properties was not possible. Biot's constant was assumed to be 1 and Pp was assumed to be hydrostatic at normal seawater density (1.02 g/cc).
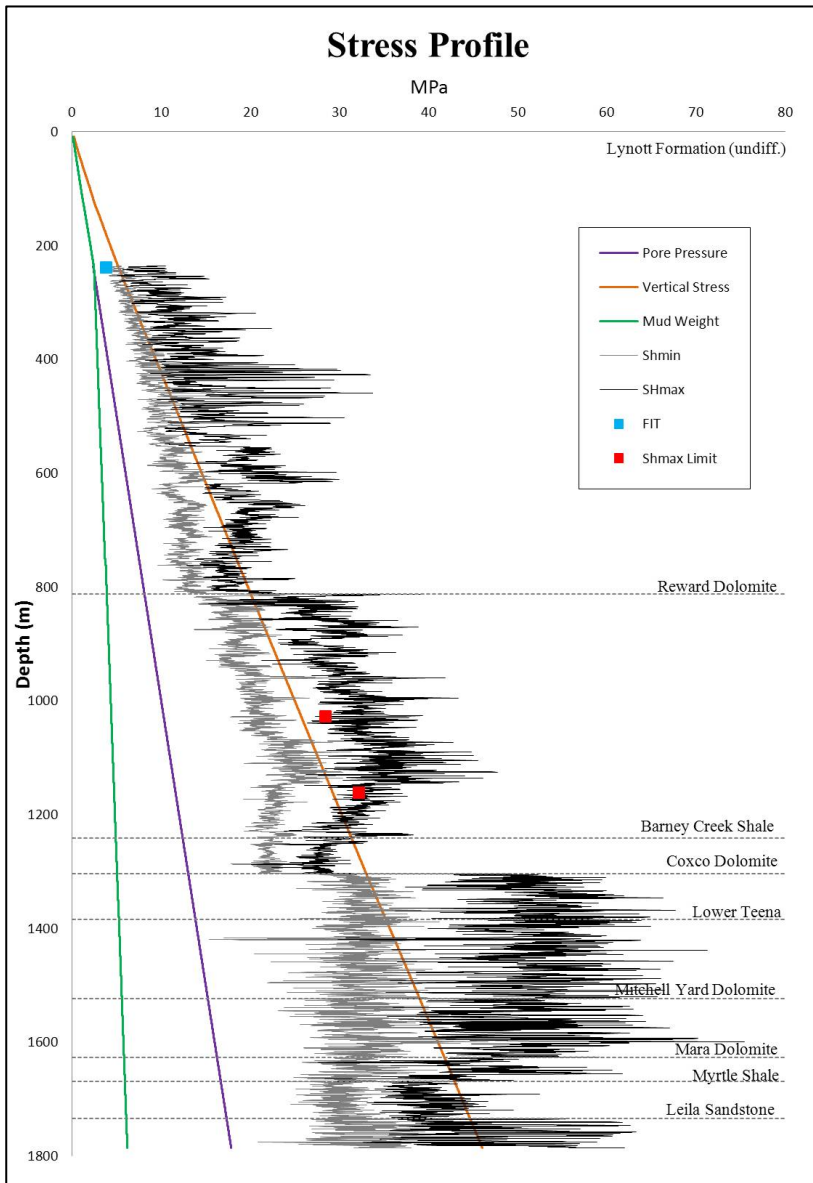

Figure 6: Cow Lagoon-1 stress profile showing formations.

Uniaxial compressive strength (UCS) of the wellbore wall was determined for Cow Lagoon-1 using Golubev & Rabinovich (1976 in Chang 2004) empirical relationship derived for limestones and dolomites (Figure 7).

The poro-elastically derived σ_h magnitude was calibrated to exceed the single FIT measurement that was made in Cow Lagoon-1 (Figure 6). Borehole breakout occurrence was used to model circumferential stresses and constrain σ_H magnitudes. Maximum constraints on σ_H magnitude at these depths is defined by the frictional limit assuming a coefficient of friction (μ) of 0.6. The derived maximum horizontal stress curve was calibrated to these points by varying the tectonic strains in the σ_h and σ_H stress directions (Figure 6).

The distribution of stresses within these units varies considerably and is fundamentally linked to the elastic properties of the sampled stratigraphy. The Leila Sandstone at the base of the well is characterized by a strike-slip stress regime with σ_H predominantly $\geq \sigma_v$. The Myrtle Shale is characterized by an extensional stress regime and this is a reflection of a high Poisson's Ratio. This is in contrast to the overlying Mara Member with a lower Poisson's Ratio which correlates with an increase of both the horizontal principal stress magnitudes to a strike-slip stress regime. The overlying Dolomites have increasingly high Young's Modulus, which correlates with higher horizontal stress magnitudes. The stress regime at the base of these formations remains strike-slip and tends towards compressional at the top of the Coxco Dolomite.

There is a significant change in the distribution of stress at the interface between the Coxco Dolomite and the Barney Creek Formation where stress magnitudes are reduced (strike-slip stress regime). Maximum horizontal stress magnitude gradually increases from the base of the overlying Reward Dolomite returning to a strike-slip stress regime. Horizontal stress magnitudes are again reduced to an extensional stress regime at the base of the Lynott Formation before becoming strike-slip above approximately 750m.
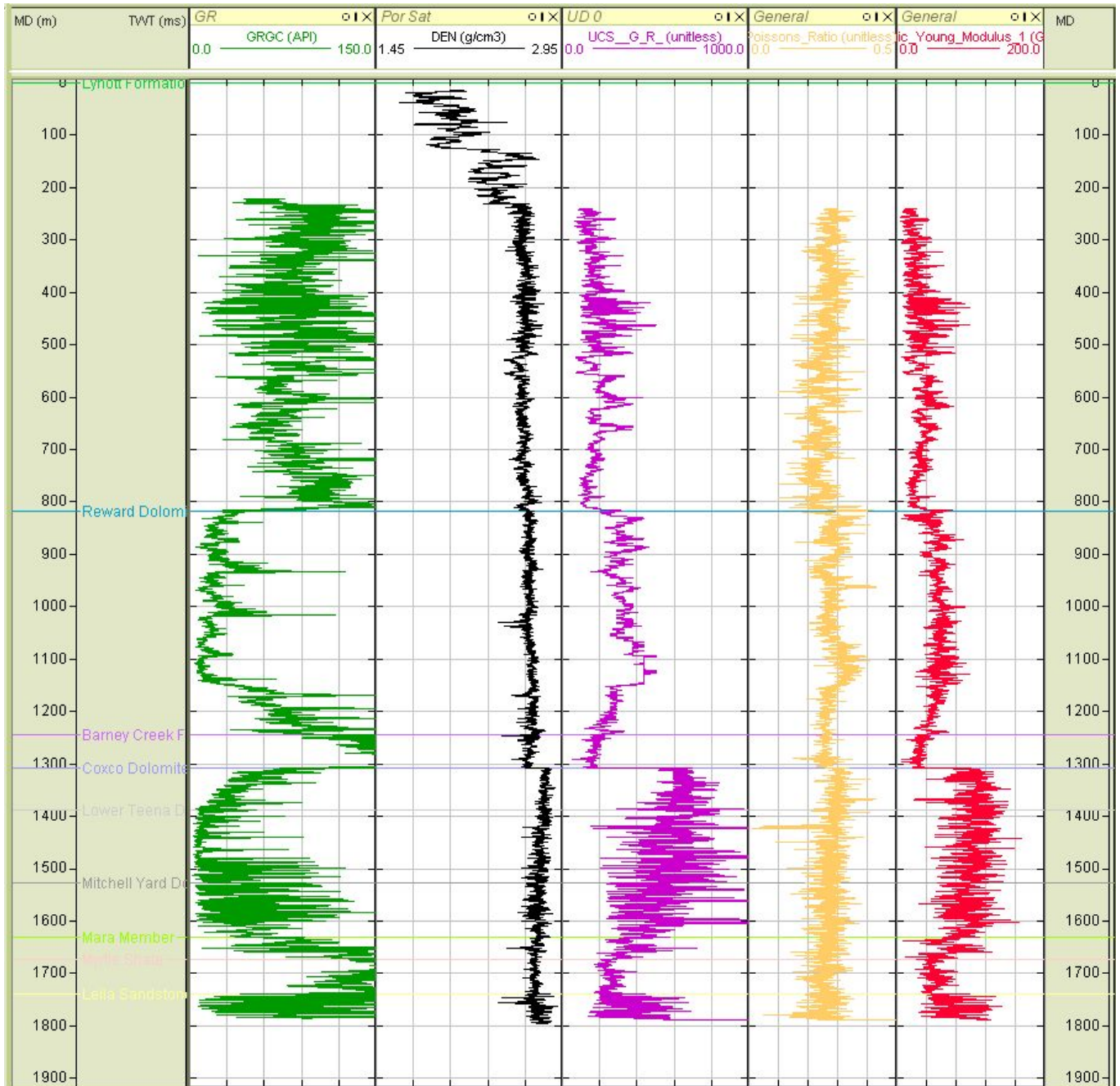
Fracture Susceptibility

Fracture susceptibility is a methodology for evaluating the relative permeability of fault and fracture orientations utilizing the Mohr diagram's representation of stress and strength (Mildren *et al*, 2002). The fracture susceptibility of a particular fracture orientation is determined by resolving the shear and normal stresses acting on the plane and calculating the pressure change required to initiate failure. This approach permits the relative ranking of fractures with respect to permeability and can identify the likely mode of failure (tensile, shear or hybrid tensile-shear) based on the relationship between the differential stress and the tensile strength.

**Figure 7: Distribution of elastic properties and rock strength within the interpreted interval of Cow Lagoon-1.**

The geomechanical model derived for Cow Lagoon-1 was used to generate fracture susceptibility models for the fracture populations observed from image log data. Fracture susceptibility models are polar diagrams of fracture poles to planes coloured by the pore pressure required to reactivate or create the fracture. The failure envelope is representative of either the intact host rock derived from the rock strength or a pre-existing fracture surface using no cohesive strength. The pressure is a measure of the permeability likelihood. Red orientations correspond to a low ΔP and higher likelihood of permeability.

Generic fracture susceptibility models were generated for Cow Lagoon-1 using calculated stress conditions and rock strengths for each formation (Figure 8). Formations with similar elastic properties were grouped for assessment. A second set of models was generated for each formation using the same stress conditions. However, failure envelopes with no cohesive strength and a coefficient of friction of 0.6 were used to represent pre-existing structural surfaces to evaluate their likelihood of reactivation (Figure 8).
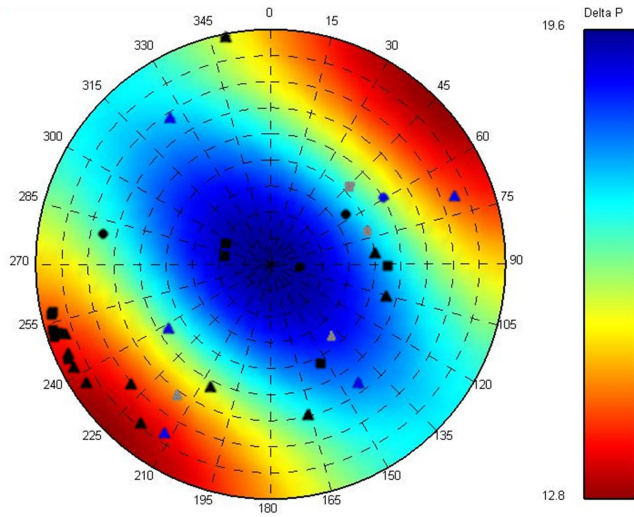
Minimum ΔP to initiate a fracture is relatively high in all formations considered, exceeding 25 MPa with the exception of the Base of the Lynott Formation (12.6 MPa). This reflects the high strength calculated for these units and implies that creation of
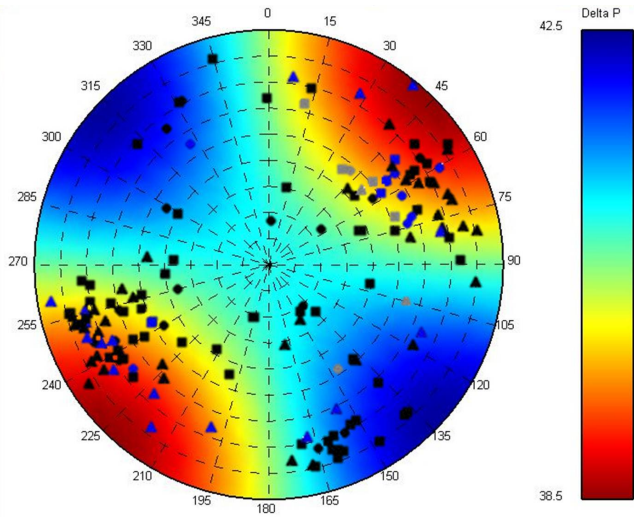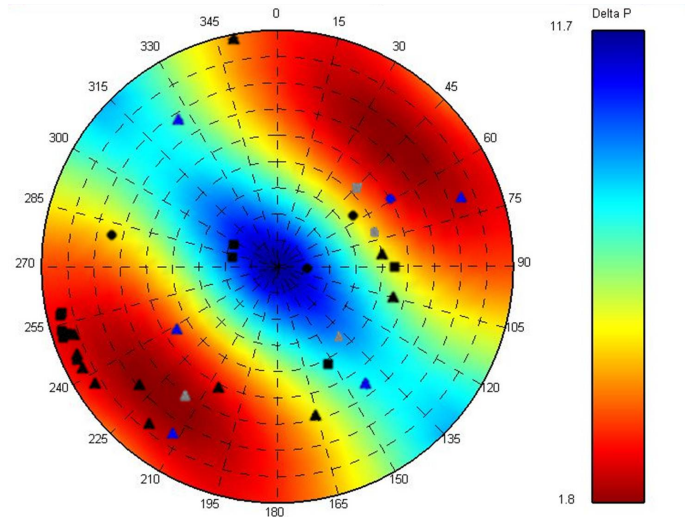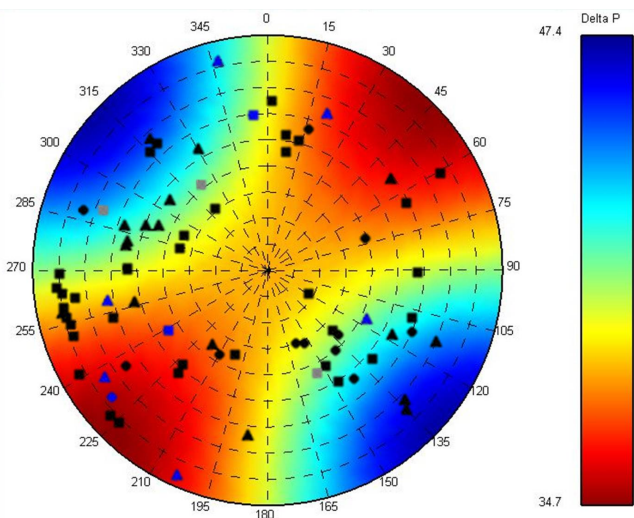
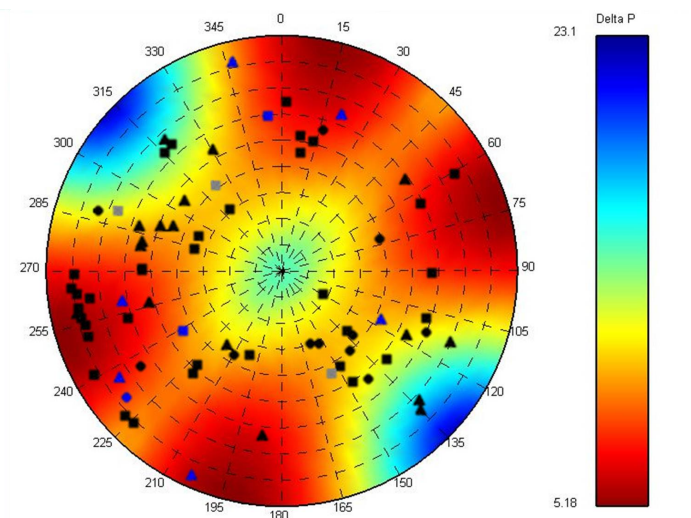A.   Upper Lynott Formation
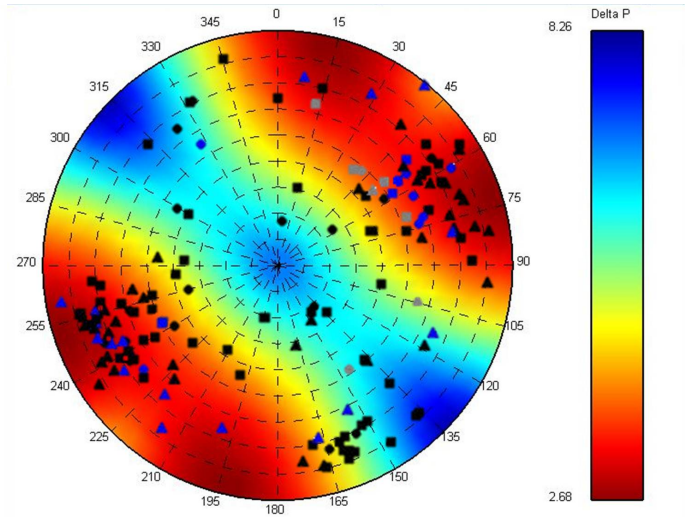
B.   Upper Lynott Formation

C.   Base Lynott Formation

D.   Base Lynott Formation

E.   Reward Dolomite

F.   Reward Dolomite

G. Barney Creek Formation

H. Barney Creek Formation

I. Teena Dolomite

J. Teena Dolomite

K. Myrtle Shale
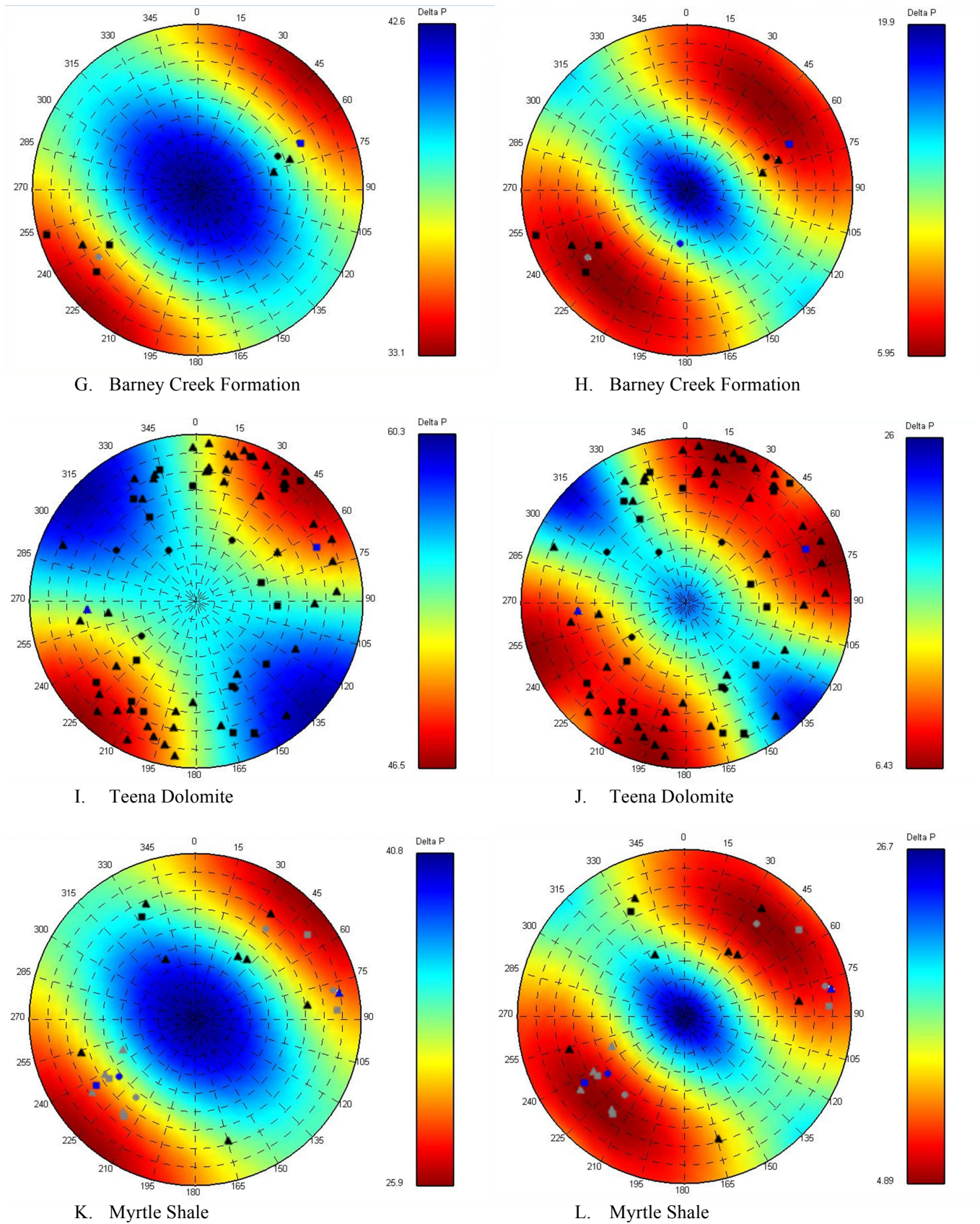
L. Myrtle Shale

Figure 8: Structural permeability plots showing scenarios assuming the host rock strength (A, C, E, G, I and K) and assuming pre-existing fractures (B, D, F, H, J and L). Fractures and faults are plotted as poles to planes and show conductive fractures (black), resistive fractures (grey) and conductive and resistive faults (blue).

new fractures under these contemporary stress conditions is unlikely. The risk of reactivating any existing fracture planes is far greater with minimum $\Delta P < 7$ MPa in each fracture susceptibility model. In fact, the risk of reactivating a fracture plane in the least favorable orientation in each model is still higher than the likelihood of creating a new fracture in the host rock. These observations imply that although many of the fractures may be enhanced at the wellbore wall due to the local stress re-distribution attributed to the borehole, many of the observed fractures are optimally oriented to be open or hydraulically conductive in the far field stress field.

Superimposed on each fracture susceptibility model are the interpreted fractures from within the relevant formations being considered. The populations of conductive faults and fractures in the Lynott Formation and the Reward Dolomite that coincide with high likelihood of structural permeability (low ΔP) also correspond with similarly oriented resistive fractures. They are also sub-parallel to significant local structural elements (Batten Fault Zone) and it is likely that they are of natural origin and permeable away from the wellbore. These units also correspond with recorded gas shows and are therefore potential targets for production.

There is significantly less fracturing in the Barney Creek Formation, although observed conductive fractures are oriented to be permeable and they correspond with a similarly oriented resistive fracture implying natural origin.

The East-West striking discontinuous fracture population (CFracD) almost exclusively occurs within the Coxco, Lower Teena and Mitchell Yard Dolomites. These fractures are sub-parallel to the σ_H orientation and occur in the formations with the highest differential stress and the highest Youngs Modulus. Very few fault surfaces were identified and although this interval has the highest observed fracture density no corresponding gas shows were identified. The high horizontal stresses within this unit, attributed to the high Young's Modulus, translate to high circumferential stresses around the wellbore wall. The likelihood of tensile failure enhancement of pre-existing surfaces is high. Enhancement of these fractures at the wellbore wall does not imply they are likely to be permeable conduits away from the wellbore wall.

Resistive natural fractures are observed within the Myrtle Shale, which is of intermediate strength and Young's Modulus. A small population of conductive fractures also exists, some of which are oriented parallel to maximum horizontal stress. This indicates they are enhanced at the wellbore and not open or permeable in the far field environment.

Conclusions

The principal objective of this study was to characterise fracture distribution, assess the permeability of these fractures and explore options for production at Cow Lagoon-1 in the McArthur Basin.

Analysis of the Cow Lagoon-1 data concludes that NNW striking fractures at approximately 150°N are critically oriented for shear reactivation in the far field stress environment, within the Upper Lynott and Reward Formations. This interval also correlates with gas encountered during drilling. Fracture susceptibility assessment shows that the risk of reactivating pre-existing fractures is far greater than initiating new fractures. The greatest susceptibility corresponds with intervals of high fault density and shear failure. These preferentially occur within units of intermediate Poisson's Ratio, low Young's Modulus and low differential and effective stress.

This study also shows that this type of analysis can be used to assess image log based fracture populations and determine the likelihood that they are features likely to be observed in the far field away from the near wellbore stress concentrations. The large population of East-West striking discontinuous fractures (CFracD) observed within the Coxco, Lower Teena and Mitchell Yard Dolomites are considered to be wellbore related and not necessarily indicative of structural permeability away from the wellbore. This is an important observation in the context of costly operations to unsuccessfully exploit what is thought to be a natural fracture set.

Hydraulic fracturing is recommended within intervals where the stress magnitudes and elastic properties meet the criteria outlined above. The presence of pre-existing fractures will enable more complex permeability networks to be established through the generation of shear and tensile fractures. This will be beneficial within intervals of low fracture density that also meet the same elastic and stress criteria. Orienting wellbores parallel to the direction of minimum horizontal stress can also optimise permeability. This is also likely to maximize intersection with pre-existing fractures.

Acknowledgements

References

Brudy, M., and Zoback, M.D., 1999. Drilling-induced tensile wall-fractures: implications for determination of in-situ stress orientation and magnitude. International Journal of Rock Mechanics and Mining Sciences 36 (1999) 191±215.

Blanton, T.L. and Olson, J.E., 1999. Stress Magnitudes from Logs: Effects of Tectonic Strains and Temperature. *SPE Reservoir Eval & Eng,* vol. 2, pg. 62-68.
Chang, C., (2004) Empirical Rock Strength Logging in Boreholes Penetrating Sedimentary Formations, Vol. 7, No. 3, p. 174-183

Edgoose, C. J., M Ahmad, Dunster, J. N. and Munson, T. J., 2013. Overview of the geology and mineral and petroleum resources of the McArthur Basin. *Northern Territory Geological Survey,* Annual Geoscience Exploration Seminar, Northern Territory.

Hillis, R.R., Mildren, S.D. and Meyer, J.J., 2000. Borehole geomechanics in petroleum exploration and development: from controlling wellbore stability to predicting fault seal integrity. *Preview*, 89, p. 31-34.

Hillis, R.R., Reynolds, S.D., 2002. CHAPTER 4 – In situ stress field of Australia. *Geological Society of Australia Special Publication 22,* p. 43-52.

Mildren , S.D., Hillis , R.R. and Kaldi , J ., 2002, Calibrating predictions of fault seal reactivation in the Timor Sea. *Australian Petroleum Production and Exploration Association Journal*, v. 42, p. 187-202.

Rawlings, D. J., 2002. Sedimentology, volcanology and geodynamics of the Redbank Package, McArthur Basin, northern Australia. *PhD thesis, University of Tasmania*.

Rawlings, D.J., Korsch, R.J., Goleby, B.R., Gibson, G.M., Johnstone, D.W. and Barlow, M., 2004. The 2002 Southern McArthur Basin Seismic Reflection Survey. *Geoscience Australia*, Record 2004/17, p. 78.

Sibson, R.H., 1996. Structural permeability of fluid-driven fault-fracture meshes. Journal of Stuctural Geology, 18, p. 1031-1042.

Zoback, M., 2007. Reservoir Geomechanics. *Cambridge University Press*.